Journal of Instrumentation

The experimental facility for the Search for Hidden Particles at the CERN SPS

Published by IOP Publishing for Sissa Medialab

Received: *November 2, 2018*
Accepted: *February 25, 2019*
Published: *March 25, 2019*

The experimental facility for the Search for Hidden Particles at the CERN SPS

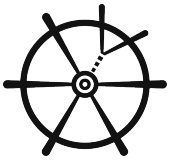

The SHiP collaboration

C. Ahdida,[44] R. Albanese,[14,a] A. Alexandrov,[14] A. Anokhina,[39] S. Aoki,[18] G. Arduini,[44] E. Atkin,[38] N. Azorskiy,[29] J.J. Back,[54] A. Bagulya,[32] F. Baaltasar Dos Santos,[44] A. Baranov,[40] F. Bardou,[44] G.J. Barker,[54] M. Battistin,[44] J. Bauche,[44] A. Bay,[46] V. Bayliss,[51] G. Bencivenni,[15] A.Y. Berdnikov,[37] Y.A. Berdnikov,[37] I. Berezkina,[32] M. Bertani,[15] C. Betancourt,[47] I. Bezshyiko,[47] O. Bezshyyko,[55] D. Bick,[8] S. Bieschke,[8] A. Blanco,[28] J. Boehm,[51] M. Bogomilov,[1] K. Bondarenko,[27,57] W.M. Bonivento,[13] J. Borburgh,[44] A. Boyarsky,[27,55] R. Brenner,[43] D. Breton,[4] R. Brundler,[47] M. Bruschi,[12] V. Büscher,[10] A. Buonaura,[47] S. Buontempo,[14] S. Cadeddu,[13] A. Calcaterra,[15] M. Calviani,[44] M. Campanelli,[53] M. Casolino,[44] N. Charitonidis,[44] P. Chau,[10] J. Chauveau,[5] A. Chepurnov,[39] M. Chernyavskiy,[32] K.-Y. Choi,[26] A. Chumakov,[2] P. Ciambrone,[15] K. Cornelis,[44] M. Cristinziani,[7] A. Crupano,„[14,d] G.M. Dallavalle,[12] A. Datwyler,[47] N. D'Ambrosio,[16] G. D'Appollonio,[13,c] J. De Carvalho Saraiva,[28] G. De Lellis,[14,d] M. de Magistris,[14,d] A. De Roeck,[44] M. De Serio,[11,a] D. De Simone,[14,d] L. Dedenko,[39] P. Dergachev,[34] A. Di Crescenzo,[14,d] N. Di Marco,[16] C. Dib,[2] H. Dijkstra,[44] P. Dipinto,[11,a] V. Dmitrenko,[38] S. Dmitrievskiy,[29] L.A. Dougherty,[44] A. Dolmatov,[30] D. Domenici,[15] S. Donskov,[35] V. Drohan,[55] A. Dubreuil,[45] J. Ebert,[8] T. Enik,[29] A. Etenko,[33,38] F. Fabbri,[12] L. Fabbri,[12,b] A. Fabich,[44] O. Fedin,[36] F. Fedotovs,[52] G. Felici,[15] M. Ferro-Luzzi,[44] K. Filippov,[38] R.A. Fini,[11] P. Fonte,[28] C. Franco,[28] M. Fraser,[44] R. Fresa,[14,i] R. Froeschl,[44] T. Fukuda,[19] G. Galati,[14,d] J. Gall,[44] L. Gatignon,[44] G. Gavrilov,[38] V. Gentile,[14,d] B. Goddard,[44] L. Golinka-Bezshyyko,[55] A. Golovatiuk,[55] D. Golubkov,[30] A. Golutvin,[52,34] P. Gorbounov,[44] D. Gorbunov,[31] S. Gorbunov,[32] V. Gorkavenko,[55] Y. Gornushkin,[29] M. Gorshenkov,[34] V. Grachev,[38] A.L. Grandchamp,[46] G. Granich,[32] E. Graverini,[47] J.-L. Grenard,[44] D. Grenier,[44] V. Grichine,[32] N. Gruzinskii,[36] A. M. Guler,[48] Yu. Guz,[35] G.J. Haefeli,[46] C. Hagner,[8] H. Hakobyan,[2] I.W. Harris,[46] E. van Herwijnen,[44] C. Hessler,[44] A. Hollnagel,[10] B. Hosseini,[52] M. Hushchyn,[40] G. Iaselli,[11,a] A. Iuliano,[14,d] V. Ivantchenko,[32] R. Jacobsson,[44] D. Joković,[41] M. Jonker,[44] I. Kadenko,[55] V. Kain,[44] C. Kamiscioglu,[49] K. Kershaw,[44] M. Khabibullin,[31] E. Khalikov,[39]

https://doi.org/10.1088/1748-0221/14/03/P03025

2019 JINST 14 P03025

G. Khaustov,[35] G. Khoriauli,[10] A. Khotyantsev,[31] S.H. Kim,[22] Y.G. Kim,[23] V. Kim,[36,37] N. Kitagawa,[19] J.-W. Ko,[22] K. Kodama,[17] A. Kolesnikov,[29] D.I. Kolev,[1] V. Kolosov,[35] M. Komatsu,[19] N. Kondrateva,[32] A. Kono,[21] N. Konovalova,[32,34] S. Kormannshaus,[10] I. Korol,[6] I. Korol'ko,[30] A. Korzenev,[45] V. Kostyukhin,[7] E. Koukovini Platia,[44] S. Kovalenko,[2] I. Krasilnikova,[34] Y. Kudenko,[31,38,g] E. Kurbatov,[40] P. Kurbatov,[34] V. Kurochka,[31] E. Kuznetsova,[36] H.M. Lacker,[6] M. Lamont,[44] G. Lanfranchi,[15] O. Lantwin,[52] A. Lauria,[14,d] K.S. Lee,[25] K.Y. Lee,[22] J.-M. Lévy,[5] V.P. Loschiavo,[14,h] L. Lopes,[28] E. Lopez Sola,[44] V. Lyubovitskij,[2] J. Maalmi,[4] A. Magnan,[52] V. Maleev,[36] A. Malinin,[33] Y. Manabe,[19] A.K. Managadze,[39] M. Manfredi,[44] S. Marsh,[44] A.M. Marshall,[50] A. Mefodev,[31] P. Mermod,[45] A. Miano,[14,d] S. Mikado,[20] Yu. Mikhaylov,[35] D.A. Milstead,[42] O. Mineev,[31] A. Montanari,[12] M.C. Montesi,[14,d] K. Morishima,[19] S. Movchan,[29] Y. Muttoni,[44] N. Naganawa,[19] M. Nakamura,[19] T. Nakano,[19] S. Nasybulin,[36] P. Ninin,[44] A. Nishio,[19] A. Novikov,[38] B. Obinyakov,[33] S. Ogawa,[21] N. Okateva,[32,34] B. Opitz,[8] J. Osborne,[44] M. Ovchynnikov,[27,55] N. Owtscharenko,[7] P.H. Owen,[47] P. Pacholek,[44] A. Paoloni,[15] R. Paparella,[11] B.D. Park,[22] S.K. Park,[25] A. Pastore,[12] M. Patel,[52] D. Pereyma,[30] A. Perillo-Marcone,[44] G.L. Petkov,[1] K. Petridis,[50] A. Petrov,[33] D. Podgrudkov,[39] V. Poliakov,[35] N. Polukhina,[32,34,38] J. Prieto Prieto,[44] M. Prokudin,[30] A. Prota,[14,d] A. Quercia,[14,d] A. Rademakers,[44] A. Rakai,[44] F. Ratnikov,[40] T. Rawlings,[51] F. Redi,[46] S. Ricciardi,[51] M. Rinaldesi,[44] Volodymyr Rodin,[55] Viktor Rodin,[55] P. Robbe,[4] A.B. Rodrigues Cavalcante,[46] T. Roganova,[39] H. Rokujo,[19] G. Rosa,[14,d] T. Rovelli,[12,b] O. Ruchayskiy,[3] T. Ruf,[44] V. Samoylenko,[35] V. Samsonov,[38] F. Sanchez Galan,[44] P. Santos Diaz,[44] A. Sanz Ull,[44] A. Saputi,[15] O. Sato,[19] E.S. Savchenko,[34] W. Schmidt-Parzefall,[8] N. Serra,[47] S. Sgobba,[44] O. Shadura,[55] A. Shakin,[34] M. Shaposhnikov,[46] P. Shatalov,[30] T. Shchedrina,[32,34] L. Shchutska,[55] V. Shevchenko,[33] H. Shibuya,[21] S. Shirobokov,[52] A. Shustov,[38] S.B. Silverstein,[42] S. Simone,[11,a] R. Simoniello,[10] M. Skorokhvatov,[38,33] S. Smirnov,[38] J.Y. Sohn,[22] A. Sokolenko,[55] E. Solodko,[44] N. Starkov,[32,33] L. Stoel,[44] B. Storaci,[47] M.E. Stramaglia,[46] D. Sukhonos,[44] Y. Suzuki,[19] S. Takahashi,[18] J.L. Tastet,[3] P. Teterin,[38] S. Than Naing,[32] I. Timiryasov,[46] V. Tioukov,[14] D. Tommasini,[44] M. Torii,[19] N. Tosi,[12] D. Treille,[44] R. Tsenov,[1,29] S. Ulin,[38] A. Ustyuzhanin,[40] Z. Uteshev,[38] G. Vankova-Kirilova,[1] F. Vannucci,[5] P. Venkova,[6] V. Venturi,[44] S. Vilchinski,[55] M. Villa,[12,b] Heinz Vincke,[44] Helmut Vincke,[44] C. Visone,[14,j] K. Vlasik,[38] A. Volkov,[32,33] R. Voronkov,[32] S. van Waasen,[9] R. Wanke,[10] P. Wertelaers,[44] J.-K. Woo,[24] M. Wurm,[10] S. Xella,[3] D. Yilmaz,[49] A.U. Yilmazer,[49] C.S. Yoon,[22] P. Zarubin,[29] I. Zarubina[29] and Yu. Zaytsev[30]

[1] *Faculty of Physics, Sofia University, Sofia, Bulgaria*

[2] *Universidad Técnica Federico Santa María and Centro Científico Tecnológico de Valparaíso, Valparaíso, Chile*

[3] *Niels Bohr Institute, University of Copenhagen, Copenhagen, Denmark*

[4] *LAL, Univ. Paris-Sud, CNRS/IN2P3, Université Paris-Saclay, Orsay, France*

[5] *LPNHE, IN2P3/CNRS, Sorbonne Université, Université Paris Diderot,F-75252 Paris, France*

[6] *Humboldt-Universität zu Berlin, Berlin, Germany*

[7] *Physikalisches Institut, Universität Bonn, Bonn, Germany*

[8] *Universität Hamburg, Hamburg, Germany*

[9] *Forschungszentumr Jülich GmbH (KFA), Jülich , Germany*

2019 JINST 14 P03025

[10] *Institut für Physik and PRISMA Cluster of Excellence, Johannes Gutenberg Universität Mainz, Mainz, Germany*
[11] *Sezione INFN di Bari, Bari, Italy*
[12] *Sezione INFN di Bologna, Bologna, Italy*
[13] *Sezione INFN di Cagliari, Cagliari, Italy*
[14] *Sezione INFN di Napoli, Napoli, Italy*
[15] *Laboratori Nazionali dell'INFN di Frascati, Frascati, Italy*
[16] *Laboratori Nazionali dell'INFN di Gran Sasso, L'Aquila, Italy*
[17] *Aichi University of Education, Kariya, Japan*
[18] *Kobe University, Kobe, Japan*
[19] *Nagoya University, Nagoya, Japan*
[20] *College of Industrial Technology, Nihon University, Narashino, Japan*
[21] *Toho University, Funabashi, Chiba, Japan*
[22] *Physics Education Department & RINS, Gyeongsang National University, Jinju, Korea*
[23] *Gwangju National University of Education,[e] Gwangju, Korea*
[24] *Jeju National University,[e] Jeju, Korea*
[25] *Korea University, Seoul, Korea*
[26] *Sungkyunkwan University,[e] Suwon-si, Gyeong Gi-do, Korea*
[27] *University of Leiden, Leiden, The Netherlands*
[28] *LIP, Laboratory of Instrumentation and Experimental Particle Physics, Portugal*
[29] *Joint Institute for Nuclear Research (JINR), Dubna, Russia*
[30] *Institute of Theoretical and Experimental Physics (ITEP) NRC 'Kurchatov Institute', Moscow, Russia*
[31] *Institute for Nuclear Research of the Russian Academy of Sciences (INR RAS), Moscow, Russia*
[32] *P.N. Lebedev Physical Institute (LPI), Moscow, Russia*
[33] *National Research Centre 'Kurchatov Institute', Moscow, Russia*
[34] *National University of Science and Technology "MISiS", Moscow, Russia*
[35] *Institute for High Energy Physics (IHEP) NRC 'Kurchatov Institute', Protvino, Russia*
[36] *Petersburg Nuclear Physics Institute (PNPI) NRC 'Kurchatov Institute', Gatchina, Russia*
[37] *St. Petersburg Polytechnic University (SPbPU),[f] St. Petersburg, Russia*
[38] *National Research Nuclear University (MEPhI), Moscow, Russia*
[39] *Skobeltsyn Institute of Nuclear Physics of Moscow State University (SINP MSU), Moscow, Russia*
[40] *Yandex School of Data Analysis, Moscow, Russia*
[41] *Institute of Physics, University of Belgrade, Serbia*
[42] *Stockholm University, Stockholm, Sweden*
[43] *Uppsala University, Uppsala, Sweden*
[44] *European Organization for Nuclear Research (CERN), Geneva, Switzerland*
[45] *University of Geneva, Geneva, Switzerland*
[46] *École Polytechnique Fédérale de Lausanne (EPFL), Lausanne, Switzerland*
[47] *Physik-Institut, Universität Zürich, Zürich, Switzerland*
[48] *Middle East Technical University (METU), Ankara, Turkey*
[49] *Ankara University, Ankara, Turkey*
[50] *H.H. Wills Physics Laboratory, University of Bristol, Bristol, United Kingdom*
[51] *STFC Rutherford Appleton Laboratory, Didcot, United Kingdom*
[52] *Imperial College London, London, United Kingdom*

2019 JINST 14 P03025

[53] *University College London, London, United Kingdom*
[54] *University of Warwick, Warwick, United Kingdom*
[55] *Taras Shevchenko National University of Kyiv, Kyiv, Ukraine*
[a] *Università di Bari, Bari, Italy*
[b] *Università di Bologna, Bologna, Italy*
[c] *Università di Cagliari, Cagliari, Italy*
[d] *Università di Napoli "Federico II", Napoli, Italy*
[e] *Associated to Gyeongsang National University, Jinju, Korea*
[f] *Associated to Petersburg Nuclear Physics Institute (PNPI), Gatchina, Russia*
[g] *Also at Moscow Institute of Physics and Technology (MIPT), Moscow Region, Russia*
[h] *Consorzio CREATE, Napoli, Italy*
[i] *Università della Basilicata, Potenza, Italy*
[j] *Università del Sannio, Benevento, Italy*

E-mail: Richard.Jacobsson@cern.ch

Abstract: The Search for Hidden Particles (SHiP) Collaboration has shown that the CERN SPS accelerator with its 400 GeV/c proton beam offers a unique opportunity to explore the Hidden Sector [1–3]. The proposed experiment is an intensity frontier experiment which is capable of searching for hidden particles through both visible decays and through scattering signatures from recoil of electrons or nuclei. The high-intensity experimental facility developed by the SHiP Collaboration is based on a number of key features and developments which provide the possibility of probing a large part of the parameter space for a wide range of models with light long-lived super-weakly interacting particles with masses up to $O(10)$ GeV/c^2 in an environment of extremely clean background conditions. This paper describes the proposal for the experimental facility together with the most important feasibility studies. The paper focuses on the challenging new ideas behind the beam extraction and beam delivery, the proton beam dump, and the suppression of beam-induced background.

Keywords: Large detector systems for particle and astroparticle physics; Dark Matter detectors (WIMPs, axions, etc.); Neutrino detectors

ArXiv ePrint: 1810.06880

2019 JINST 14 P03025

Contents

2019 JINST 14 P03025

1 Introduction

Given the absence of direct experimental evidence for Beyond the Standard Model (BSM) physics at the high-energy frontier and the lack of unambiguous experimental hints for the scale of new physics in precision measurements, it is plausible that the shortcomings of the Standard Model (SM) may have their origin in new physics only involving very weakly interacting, relatively light particles. Even in BSM scenarios associated with high mass scales such as in supersymmetry, many models contain light particles with suppressed couplings [4]. Considering the well-established observational evidence for a Hidden Sector in the form of Dark Matter, the structure and the phenomenology of the Hidden Sector may be more complex than just sourcing gravitational effects in the Universe. Non-minimal models of the Hidden Sector introduce various interactions and multiple types of hidden matter states charged only under the hidden interactions, as well as various types of portal interactions between the visible sector of ordinary matter and the Hidden Sector ([2, 5–10] and references therein).

As a consequence of the extremely feeble couplings for the portal interactions and the typically long lifetimes for the portal mediators, the low mass scales for hidden particles are far less constrained than the visible sector [2, 10]. In several cases, the present experimental and theoretical constraints from cosmology and astrophysics indicate that a large fraction of the interesting parameter space was beyond the reach of previous searches, but is open and accessible to current and future

facilities. While the mass range up to the kaon mass has been the subject of intensive searches, the bounds on the interaction strength of long-lived particles above this scale are significantly weaker.

Experimentally, the opportunity presents itself as an exploration at the intensity frontier with largest possible luminosity to overcome the very feeble interactions, and the largest possible acceptance to account for the typically long lifetimes. Beam-dump experiments are potentially superior to collider experiments in the sensitivity to GeV-scale hidden particles with their luminosities being several orders of magnitude larger than at colliders. The large forward boost for light states, giving good acceptance despite the smaller angular coverage and allowing efficient use of filters against background between the target and the detector, makes the beam-dump configuration ideal for searching for new particles with long lifetimes.

The recently proposed Search for Hidden Particles (SHiP) beam-dump experiment [1] at the CERN Super Proton Synchrotron (SPS) accelerator is designed to both search for decay signatures by full reconstruction and particle identification of SM final states and to search for scattering signatures of Light Dark Matter by the detection of recoil of atomic electrons or nuclei in a heavy medium. Since the hidden particles, such as dark photons, dark scalars, heavy neutral leptons, and axion-like particles, are expected to be predominantly accessible through the decays of heavy hadrons and in radiative processes, the SHiP Collaboration has proposed an experimental facility which maximises their production and the detector acceptance while providing an extremely clean background environment. This paper focuses on describing the experimental facility.

The proposal for the facility is based on a set of key themes. Firstly, the full exploitation of the SPS accelerator with its present performance allows producing up to $2 \cdot 10^{20}$ protons on target (section 3.1) in five years of nominal operation without affecting the operation of the Large Hadron Collider (LHC), and while maintaining the current level of beam usage for fixed-target facilities and test beam areas. The combination of the intensity and the 400 GeV beam energy of the SPS proton beam produces yields of different light hidden sector particles which exceed those of existing or approved future facilities [3]. At the same time, it has been found that the beam induced background flux at 400 GeV is manageable with the help of a hadron absorber and a muon shield system (section 5.1). Secondly, the unique feature of slow extraction of a de-bunched beam over a timescale of around a second (section 3.2) allows a tight control of combinatorial background, and allows diluting the large beam power deposited on the proton target both spatially and temporally.

A set of innovative technological developments makes it possible to fully profit from these features. Several new techniques to improve the beam losses and irradiation inherent with slow beam extraction have been proposed and studied (section 3.2). Improvements in these areas are also of great interest to the existing CERN fixed target programs. The preliminary design of a long, complex, high-density primary proton target has been carried out (section 4.1). This target should be capable of coping with the large beam energy, and at the same time maximising the production of charm and beauty hadrons, and the production and interactions of photons, while minimising the production of neutrinos from pions and kaons. A yield of $O(10^{18})$ charmed hadrons and $O(10^{20})$ photons above 100 MeV are expected in five years of nominal operation. The feasibility of a target complex (section 4.2) which houses the proton target together with the associated services and remote handling, fully compatible with the radiation protection and environmental considerations, has been studied in detail. Furthermore, a new type of beam splitter magnet (section 3.4), which allows switching the beam to a short new transfer line to the SHiP experimental facility, while

2019 JINST 14 P03025

keeping all of the current experimental facilities in the CERN North Area operational, has been developed. The experimental configuration includes a unique design of a muon shield (section 5.1) based on magnetic deflection to reduce the flux of muons by six orders of magnitude in the detector acceptance. A $\sim 1700\,\mathrm{m}^3$ experimental vacuum chamber (section 5.2), kept at a pressure of 1 mbar, allows suppressing residual neutrino-induced background.

Currently, CERN has no high-intensity experimental facility which is compatible with the full power of the SPS. CERN's North Area has a large space next to the SPS beam transfer lines which is for the most part free of structures and underground galleries, and which could accommodate the proposed facility. In addition, this facility is being designed with future extensions in mind.

At the energy of the SPS, the fully leptonic decays of the D_s mesons are the principal source of tau neutrinos, with an expectation of $O(10^{16})$ tau neutrinos in five years of nominal operation. Thus, while the requirements for the experimental facility for the hidden particle search makes it unsuitable for neutrino oscillation physics, the setup allows studying interactions of tau and anti-tau neutrinos at unprecedented precision. With a ten-tonne ν-target placed in front of the vacuum volume and equipped with suitable detectors, about $3 \cdot 10^4$ ($2 \cdot 10^4$) interactions of tau (anti-tau) neutrinos are expected within the geometrical acceptance. The first direct observation of the anti-tau neutrino and the measurement of tau neutrino and anti-tau neutrino cross-sections are among the physics goals of the proposed experiment. As charm hadron decays are also a source of electron and muon neutrinos, SHiP will also be able to study neutrino-induced charm production from all flavours with a dataset which is more than one order of magnitude larger than those collected by previous experiments.

2 Experimental set-up

The experimental requirements, as dictated by the phenomenologies of the different Hidden Sector models, are very similar. This allows the design of a general-purpose layout based on a global optimisation of the experimental facility and of the SHiP detector. Figure 1 shows an overview of the experimental facility from the proton target to the end of the Hidden Sector detector. The main challenges concern the requirement of a highly efficient reduction of the very large beam-induced background, and an efficient and redundant tagging of the residual background down to below 0.1 events in the projected sample of $2 \cdot 10^{20}$ protons on target. Despite the aim to cover long lifetimes, the sensitive volume should be situated as close as possible to the proton target due to the relatively large transverse momentum of the hidden particles resulting from the limited boost of the heavy hadrons (figure 2). The minimum distance is only constrained by the need of a system to absorb the electromagnetic radiation and hadrons emerging from the proton target and to reduce the beam-induced muon flux.

The proton target, described in section 4.1, is followed by a 5 m long hadron absorber. The physical dimensions of the absorber are mainly driven by the radiological requirements. In addition to absorbing the hadrons and the electromagnetic radiation, the iron of the hadron absorber is magnetised over a length of 4 m. The applied dipole field makes up the first section of the active muon shield (section 5.1) which is optimised to sweep out of acceptance the entire spectrum of muons up to $350\,\mathrm{GeV}/c$. The remaining part of the muon shield follows immediately downstream

2019 JINST 14 P03025

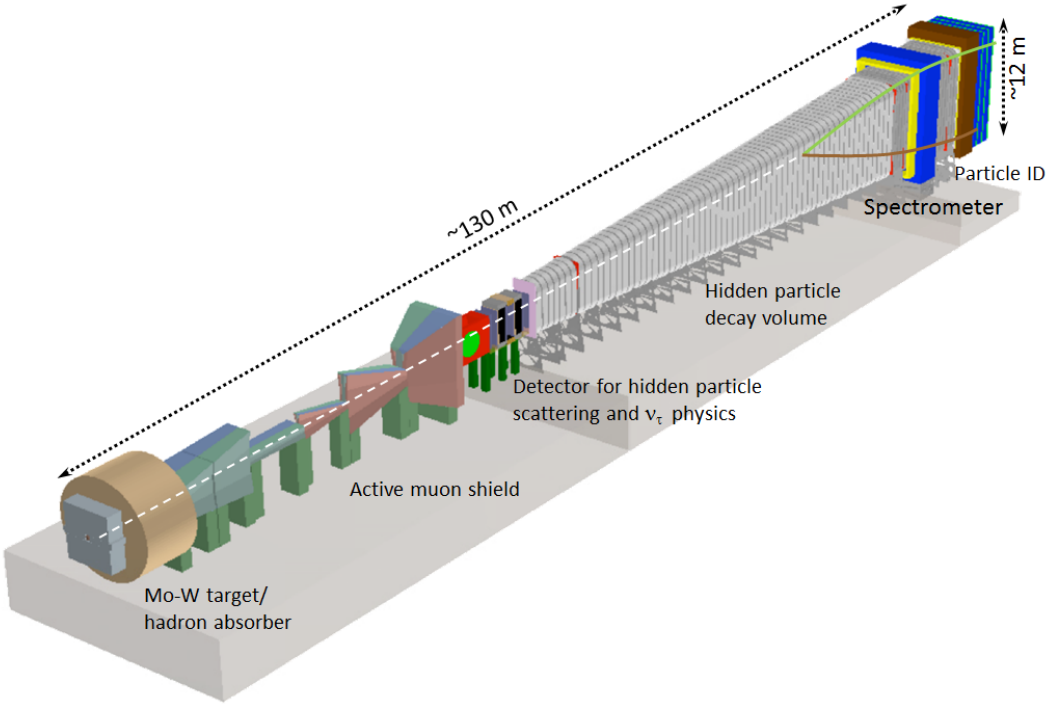

Figure 1. Overview of the target and experimental area for the SHiP detector as implemented in the physics simulation.

of the hadron absorber in the experimental hall and consists of a chain of magnets which extends over a length of ~ 40 m.

The SHiP experiment incorporates two complementary apparatuses. The detector system immediately downstream of the muon shield is optimised both for recoil signatures of hidden sector particle scattering and for neutrino physics. It is based on a hybrid detector similar to what was developed by the OPERA Collaboration [11] with alternating layers of nuclear emulsion films and electronic trackers, and high-density ν-target plates. In addition, the detector is located in a magnetic field for charge and momentum measurement of hadronic final states. The detector ν-target mass totals $O(10)$ tonnes. The emulsion spectrometer is followed by a muon identification system. This also acts as a tagger for interactions in the muon filters which may produce long-lived neutral mesons entering the downstream decay volume and whose decay may mimic signal events.

The second detector system aims at measuring the visible decays of Hidden Sector particles to both fully reconstructible final states and to partially reconstructible final states with neutrinos. The detector consists of a 50 m long decay volume (section 5.2) followed by a large spectrometer with a rectangular acceptance of 5 m in width and 10 m in height. The length of the decay volume is defined by maximising the acceptance to the hidden particle decay products (figure 2) given the transverse size of the spectrometer. In order to suppress the background from neutrinos interacting in the fiducial volume, it is maintained at a pressure of $O(10^{-3})$ bar. The spectrometer is designed to accurately reconstruct the decay vertex, the mass, and the impact parameter of the hidden particle trajectory at the proton target. A set of calorimeters and muon stations provide particle identification. The system is optimised to detect as many final states as possible in order to be sensitive to, and

2019 JINST 14 P03025

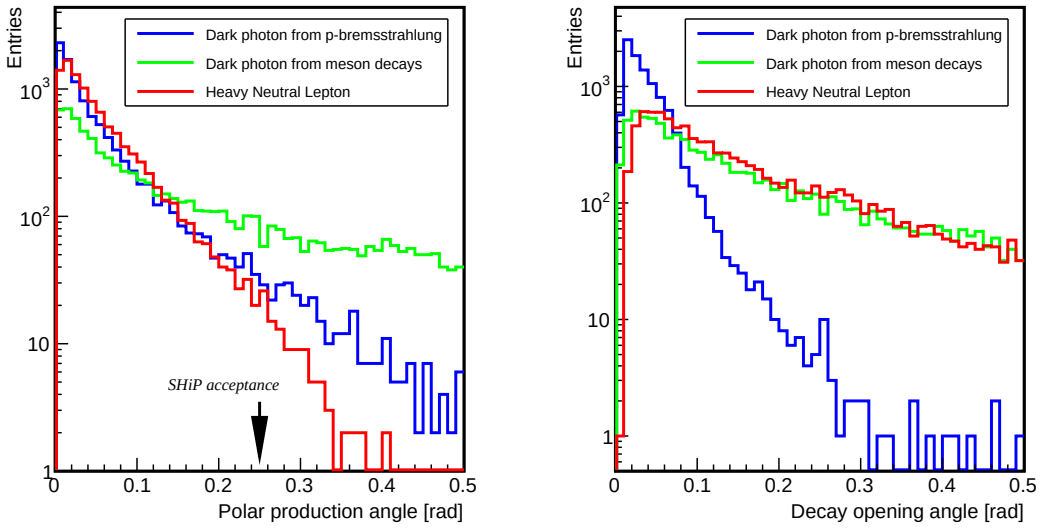

Figure 2. (Left) Polar production angle with a beam momentum of 400 GeV/c for dark photons (A) produced in proton bremsstrahlung (m_A = 2.0 GeV/c^2) and in meson decays (m_A = 0.9 GeV/c^2), and for heavy neutral leptons (HNL) (m_{HNL} = 1.0 GeV/c^2) from decays of charm hadrons. The arrow indicates the acceptance of the SHIP fiducial volume, given by the transverse size of the decay volume (Right) Decay opening angles for two-body decays of the same three cases. The geometry of the decay volume has been optimized given the aperture of the spectrometer and the hidden particle kinematics.

discriminate between, a very wide range of models. A dedicated timing detector with $\sim$ 100 ps resolution provides a measure of coincidence in order to reject combinatorial backgrounds. The decay volume is surrounded by background taggers to identify neutrino and muon inelastic scattering in the vacuum vessel walls which may produce long-lived neutral SM particles, such as K_L etc. The muon shield and the SHiP detector systems are housed in a $\sim$ 120 m long underground experimental hall at a depth of $\sim$ 15 m. To minimise the background induced by the flux of muons and neutrinos interacting with material in the vicinity of the detector, no infrastructure systems are located on the sides of the detector, and the hall is 20 m wide along the entire length.

Figure 3 shows an overview of the civil engineering required for the experimental facility for SHiP. All civil engineering works are fully located within existing CERN land on the Prevessin campus. This location is very well suited to house the experimental facility, owing to the stable and well understood ground conditions, accessible services and very limited interference with existing buildings, galleries and road structures. By maintaining the entire beam line horizontal and at the same level as the existing splitter region at the end of the SPS extraction line, the experimental hall is conveniently situated at a depth of about 15 m, which is compatible with the requirements from radiation protection while still allowing easy direct access from above without a shaft.

3 Proton beam

The proposed implementation of the SHiP experimental facility is based on minimal modifications to the SPS complex and a maximum use of the existing accelerator and beam lines. Figure 4 shows

2019 JINST 14 P03025

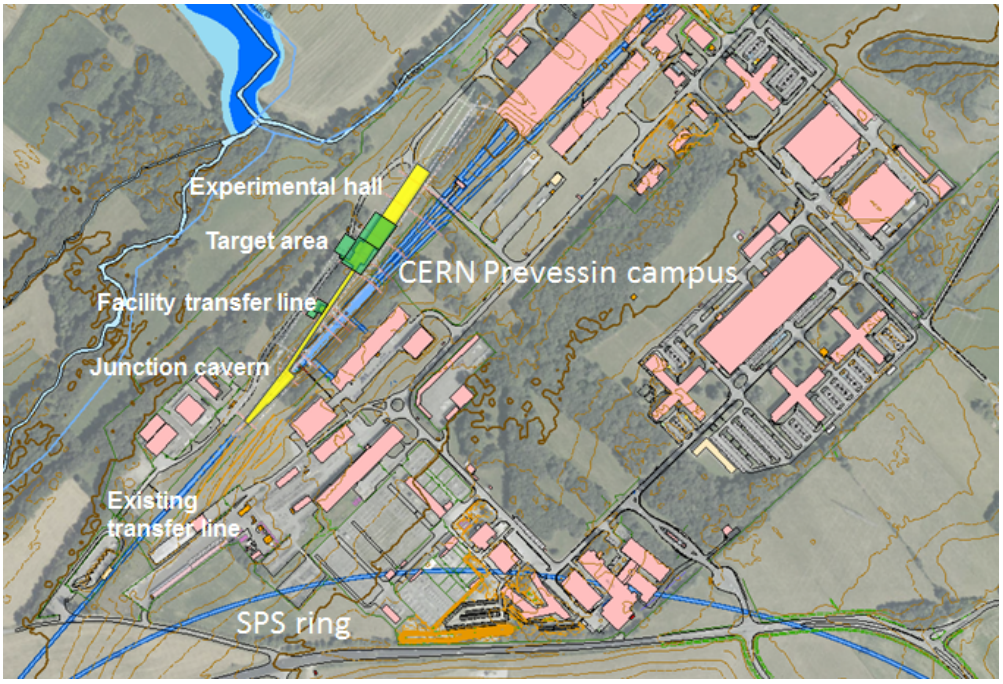

Figure 3. Overview of the required civil engineering for the proposed experimental facility for SHiP on the CERN Prevessin campus. The beam-axis is at a depth of about 10 m which allows trenching the entire complex from the surface. New or reworked construction in yellow (underground) and green (surface); existing tunnels in blue.

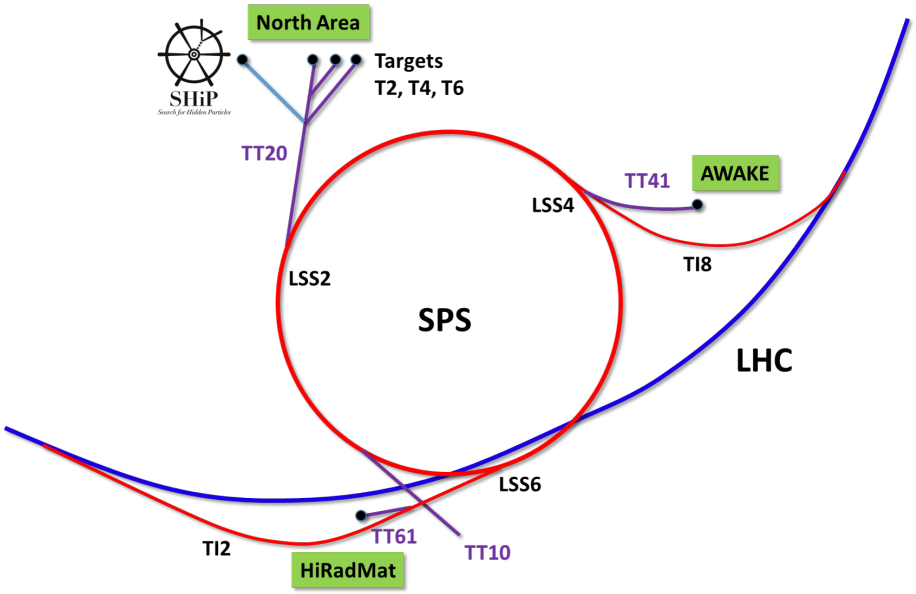

Figure 4. Overview of the SPS accelerator complex. The SHiP experimental facility is located in the North Area and shares the TT20 transfer line with the fixed target programs.

2019 JINST 14 P03025

schematically the proposed location of the experimental facility at the CERN North Area site. The facility shares about 600 m of the existing TT20 transfer line with the other North Area facilities.

At the SPS, the most favourable experimental conditions for SHiP are obtained with a proton beam momentum of around 400 GeV/c. Based on the SPS in its current state and in view of its past performance, a nominal beam intensity of $4 \cdot 10^{13}$ protons on target per spill is assumed for the design of the experimental facility and the detector.

In order to reduce the probability of combinatorial background events from residual muons entering the detector decay volume and to respect the limits on the instantaneous beam power deposited in the proton target, SHiP takes advantage of the SPS slow extraction used to provide beam to the CERN North Area through the Long Straight Section 2 of the SPS. The minimum SPS cycle length which is compatible with these requirements is 7.2 s. A beam cycle with a slow extraction of around one second has already been demonstrated in the studies for the experimental facility for SHiP (figure 5).

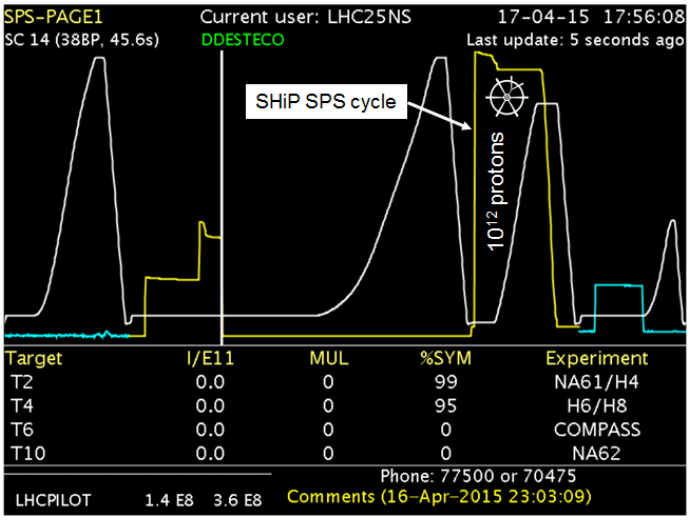

Figure 5. First slow beam extraction tests from the SPS for SHiP with the specific length of about 1 s. The tests were performed at low intensity of about 10^{12} protons/s. The yellow line represents the proton beam intensity in the SPS and the white line represents the SPS beam energy.

3.1 Achievable protons on target and beam sharing

The SHiP operational scenario is based on a similar fraction of beam time as the recently completed CERN Neutrinos to Gran Sasso (CNGS) program, and assumes the operational performance of the SPS in recent years [12]. Compatibility with the existing North Area program is important, and figure 6 shows the number of protons on the current North Area targets as a function of the number of protons on the SHiP proton target for 217 days of physics, corresponding to the situation for the 2011 run. It has been assumed that 10% of the SPS scheduled physics time is devoted to run LHC pilot cycles and another 10% to run LHC nominal cycles. The assumed sharing delivers an annual yield of $4 \cdot 10^{19}$ protons on target to the SHiP experimental facility and a total of $1 \cdot 10^{19}$ to the other physics programs at the CERN North Area. The physics sensitivities of the experiment are

2019 JINST 14 P03025

calculated based on acquiring a total of $2 \cdot 10^{20}$ protons on target which may thus be achieved in five years of nominal operation.

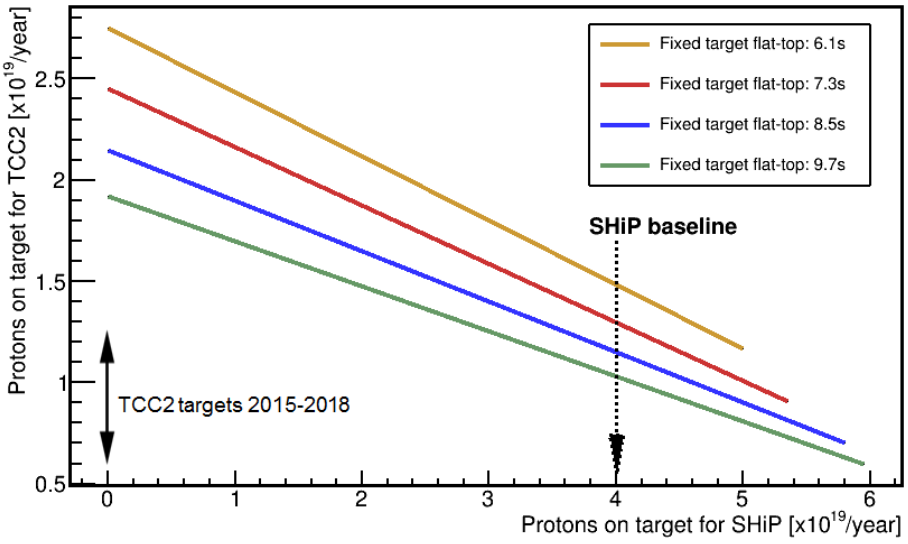

Figure 6. The expected number of protons on the current North Area targets (TCC2) as a function of the number of protons on target for the SHiP experimental facility with a 1.2 s spill length. The plot shows the performance for different spill durations for the current fixed target facilities between 6.1–9.7 s. The range of the numbers of protons per year delivered to the North Area targets in the years 2015–2018 is indicated. The preferred working point for SHIP is indicated by "SHiP baseline".

3.2 Extraction beam loss and activation

The slow extraction from the SPS exploits a third-order resonance to achieve a controlled continuous amplitude growth of the transverse oscillations of the circulating protons. The amplitudes grow over several tens of thousands of turns until a slice of the beam crosses the wires of the electrostatic septa, and is guided into the TT20 beam line aperture continuously, as shown in figure 7, until the circulating beam in the SPS is completely extracted. The field wires have finite width and inevitably intercept a fraction of the beam, leading to beam losses of the order of 2% of the total intensity. This is an important difference with respect to CNGS operation, which used essentially loss-free fast extraction.

In addition to the increased risk of sparking and damage to the wires due to heating and vacuum pressure rise, the main consequences of beam loss are radio-activation of the extraction region, accumulated radiation damage to sensitive equipment and cables, and the increased cool-down times in case of interventions for repair or maintenance. Activation and personnel dose is already a serious issue in the SPS, and currently reach operational limits with around $1.2 \cdot 10^{19}$ protons slowly extracted per year.

To extrapolate to the operation of the experimental facility for SHiP, the experience from operating the West Area Neutrino Facility (WANF) has been studied. Approximately half of the total integrated number of protons foreseen for SHiP was extracted to WANF with fast-slow (half-integer) extraction during a five-year period at the end of the 1990's. More recent experience of

2019 JINST 14 P03025

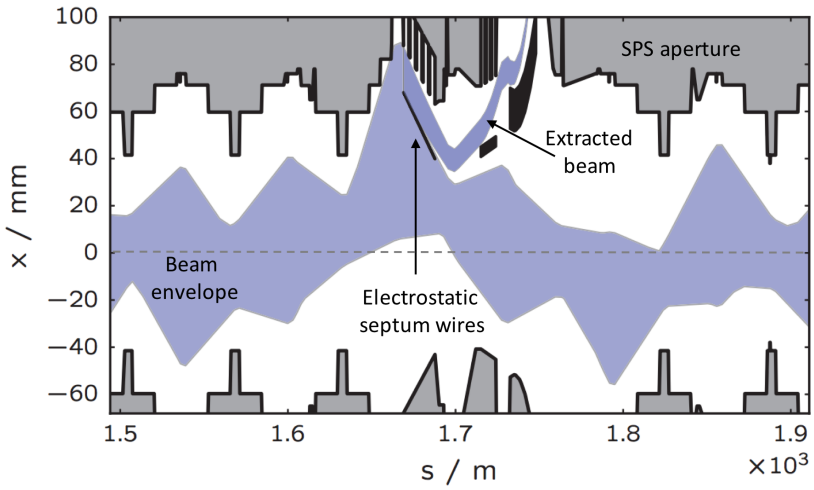

Figure 7. Envelope of the circulating and the extracted beam along the SPS extraction region, showing the machine aperture and the wires of the electrostatic septum. The passive diffuser or bent crystal are located just upstream of the electrostatic septum to reduce the density of protons impacting the wire.

sending beam to the North Area has also been considered, e.g. over $2 \cdot 10^{19}$ protons were slowly extracted to the North Area during 2007. The studies show that a factor of four decrease in the potential radiation dose to personnel is required to achieve the SHiP baseline intensity of $4 \cdot 10^{19}$ protons on target per year. This improvement will need to come from a combination of reduced beam loss, reduced activation per lost proton, and improved or remote interventions.

Extraction losses have been improved already by increasing the stability of the extraction with the help of a feed-forward system on the main quadrupole current to compensate for the ripple induced by the main electricity grid. Also, the septum wires are regularly realigned with the help of improved instrumentation and algorithms. However, a significant decrease (i.e. a factor two or more) can only be expected with substantial changes to the extraction dynamics. Studies involving two techniques based on coherent and incoherent scattering of the protons upstream of the septum (figure 7), that would otherwise hit the septum wires, are currently being tested, along with ways of modifying the transverse phase space distribution to reduce particle density at the wires.

The first technique is based on a passive beam scattering device. It consists of a short, thin blade of a high-Z material located upstream of the electrostatic septum wires. The blade intercepts a thin slice of the beam in order to generate an angular spread which reduces the transverse beam density at the wires, resulting in an overall reduction of the beam losses. Simulations show that this technique could bring up to a factor two improvement (figure 8). The device is also straightforward to deploy and operate. A prototype diffuser to benchmark the simulations with experiment is being designed and built. It will be installed in the SPS Long Straight Section 2 (LSS2 in figure 4) and tested with beam in 2018.

The second technique employs a thin bent crystal placed upstream of the septum in order to channel away the misdirected protons into the extraction aperture. Since the channeling is very sensitive to the angular alignment of the crystal, the efficiency of this technique depends strongly on the angular spread of the beam and the orbit stability. A proof-of-principle experiment with

2019 JINST 14 P03025

coasting beam has already demonstrated [13] that beam can be extracted into the TT20 transfer line using a bent crystal.

Both the crystal-assisted slow extraction and the diffuser rely on stable conditions and an accurate alignment of the septum wires and the scattering device. A movement of the extraction separatrix in position and more importantly angle is, however, inherent to the SPS extraction mechanism optimised for low beam loss. Use of a dynamic extraction bump could compensate in real-time for these changes in the closed orbit. This could also permit a faster realignment of the beam with the septa, instead of the time-consuming mechanical realignment of the septa.

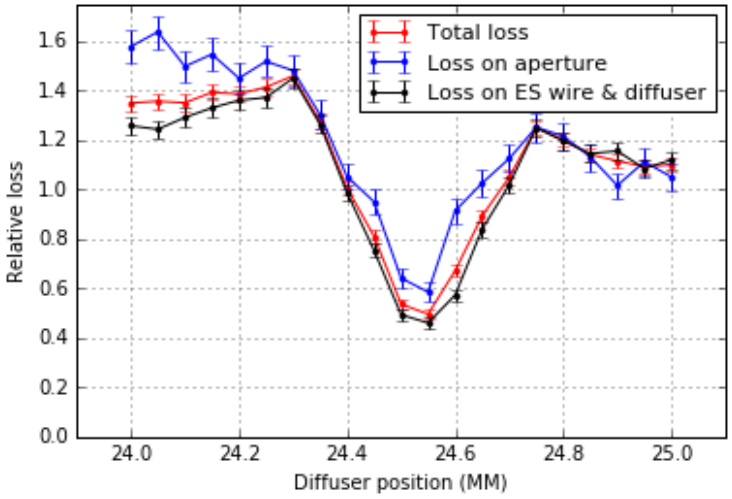

Figure 8. Relative loss of protons in arbitrary units as a function of the transverse position from simulation of a 3 mm long, 0.24 mm wide tungsten-rhenium diffuser. The sum of the loss on the diffuser and the electro-static septum (ES) wires is lower than the total loss with ES wires alone, because the scattering from the diffuser reduces the particle density at the ES sufficiently to result in an overall loss reduction. A factor two improvement is obtained for the optimal position.

A final set of studies focuses on manipulation of the transverse phase-space distribution, using either higher-order multipole magnets or a pair of septum elements in which the configuration of the conductor and magnetic material is used to separate the high-field region from the zero-field region without intervening physical material ("massless septa"), to reduce the particle density at the septum wires without increasing losses elsewhere in the extraction system. These approaches are being studied in simulation and proof-of-principle measurements have been planned for 2018. First studies of combining these techniques with the diffuser, or the crystal, indicate that it can potentially improve the loss reduction well beyond a factor two.

The different mitigation techniques are also complemented by studies of alternative materials for construction of septum sub-systems like titanium or carbon nanotubes to reduce activation, and developments of machine assisted intervention techniques.

3.3 Spill harmonic content

Suppression of combinatorial background from residual muons produced in the SHiP proton target rely on determining the time coincidence of the reconstructed tracks in the SHiP spectrometer with

the help of a timing detector. The requirement on time resolution is derived from the likelihood of coincidental muons. The likelihood is directly related to the proton interaction rate in the target, which should have minimal variations. The baseline beam parameters and the average residual muon flux in the detector acceptance requires a timing detector with a time resolution of $O(100)$ ps. Rejection of combinatorial background is thus one of the main drivers for a highly uniform extraction of the spill.

In 2017 sample spills were generated with the SHiP beam cycle, with the encouraging result that the spill harmonic content is not worse than for the longer spills used for the North Area. Contributions are dominated at low frequency by the effect of harmonics on the main electricity grid affecting the extraction beam dynamics. To this end, improvements of the stability of the slow extraction are also aiming at improving the uniformity of the spill structure. At higher frequencies the residual radio frequency structure of the beam dominates.

3.4 Beam line to proton target

The location of the SHiP proton target in the North Area allows the re-use of about 600 m of the present TT20 transfer line, which has sufficient aperture for the slow-extracted beam at 400 GeV/c. The new dedicated beam transfer line to the experimental facility for SHiP branches off at the end of the TT20 transfer line with the help of a set of newly proposed bi-polar splitter magnets which replaces the existing ones. The new magnets allow both maintaining the present function of splitting the beam between the proton target for the experimental area currently hosting the COMPASS experiment [14] and the rest of the existing North Area facilities, and to alternatively switch the entire spill to the dedicated transfer line for SHiP, on a cycle-by-cycle basis. The present magnet is an in-vacuum Lambertson septum with a yoke machined from solid iron, with the coil based on a water-cooled lead of copper with an insulation of compacted MgO powder [15]. For the new magnets a laminated yoke is required in order to rapidly perform the polarity switch between SPS cycles, which implies ramping the field reliably in about 2 s. The new magnets, shown in figure 9, must also have a larger horizontal aperture, as the beam is deflected to different sides of the magnet axis for SHiP and for North Area operation. R&D and prototyping of the laminated yoke is underway to study the very tight mechanical tolerances required in the septum region in order to maintain low beam losses. Similar MgO coil technology as used in the existing splitter will provide the required radiation resistance.

A 380 m long new section of beam line is needed, which is matched to the existing TT20 transfer line (figure 10) and which brings the beam up to the new target complex. A preliminary design has been made which exploits 17 standard SPS warm bending magnets, running at a conservative field of 1.73 T producing an angular beam deflection of 8 mrad each, to increase as much as possible the distance between the new and existing beam lines. A maximum deflection angle to exit from the tunnel of the existing beam line is beneficial to reduce the longitudinal extent of the civil engineering works in the crucial junction region. The bending dipoles downstream of the splitter are grouped into a single dipole unit as early as possible, with four subsequent standard SPS half-cells of four dipoles, each separated by a quadrupole. The powering scheme for the TT20 transfer line remains largely unchanged up to the switch element with cycle-to-cycle rematching of the last nine quadrupoles before the splitter and steering, to allow the entire beam cross-section to pass

2019 JINST 14 P03025

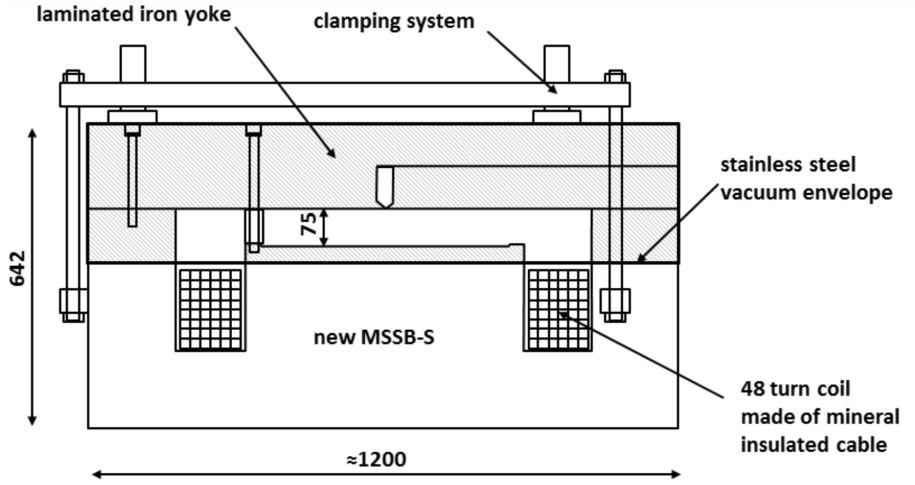

Figure 9. Cross-section of the new "MSSB-S" splitter magnet. The cycle-to-cycle polarity switching requires a laminated iron yoke. The 7.5 mm beam gap is made significantly wider than in the original splitter and extends to both sides of the septum to accommodate both the deflection of the SHiP beam to one side and alternatively splitting the beam between the other North Area facilities on the other side. All dimensions are in mm.

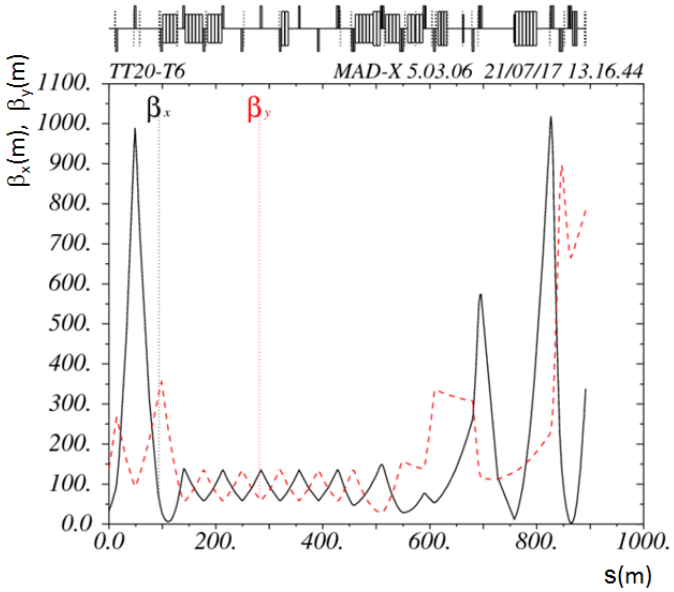

Figure 10. Optics shown by the beta function in the horizontal (black solid line) and vertical plane (red dashed line) along the entire length of the beam line from the SPS extraction (s = 0 m) in LSS2 to the SHiP proton target located at around s = 900 m. The new section of beam line is matched to the existing TT20 line to give the required beam size at the target.

through the dipole aperture with very low losses. The quadrupoles in TT20 are already laminated and suited to cycle-to-cycle switching.

For the new beam line, around six new corrector dipoles are assumed. In addition, five standard SPS quadrupole magnets will be required to control the vertical beam size through the dipole apertures, and provide flexibility and tunability of the beam spot size and dispersion at the proton target. In order to produce sufficient dilution of the beam power in the SHiP proton target, the slow extraction is combined with a beam spot of at least 6 mm root-mean square in both planes and a large sweep of the beam over the target surface. The beam sweep is implemented with two orthogonal kicker magnets located after the last bending dipole magnet at 120 m upstream of the target, with Lissajous powering functions to produce a circular sweep. With a free drift length for the beam of about 120 m and a bending angle of 0.25 mrad per plane, it is possible to achieve a sweep radius of 30 mm. Since the survival of the proton target relies critically on the beam dilution, the SPS beam is interlocked with the beam dilution system and the instantaneous loss rate at the target.

The overall layout and clearances allow civil engineering to take place along the entire experimental facility starting from the middle of the new transfer line and up to the end of the experimental hall during beam operation for the other North Area facilities.

4 Proton target and target complex

4.1 Design constraints for the proton target

The physics scope of the SHiP experiment requires a proton target which maximises the production of D and B mesons, and photons. At the same time, the proton interactions give rise to copious direct production of short-lived meson resonances, as well as pions and kaons. While a hadron absorber of a few meters of iron is sufficient to absorb the hadrons and the electromagnetic radiation emerging from the target, the decays of the pions, kaons and short-lived meson resonances result in a large flux of muons and neutrinos. In order to reduce the flux of neutrinos, in particular the flux of muon neutrinos and the associated muons, the pions and kaons should be stopped as efficiently as possible before they decay. The target should thus be made of a material with the highest possible atomic mass and atomic charge. It should be sufficiently long to intercept virtually all of the proton intensity and to contain the majority of the hadronic shower with minimum leakage. Simulation [16] shows that re-interactions of primary protons and interactions of secondaries produced in the nuclear cascades also contribute with a significant amplification of the signal yields. For instance, in the case of charm production, the cascade processes contribute by more than doubling the yield as compared to what is expected from only the primary proton-nucleus interactions.

The very high instantaneous beam power of ~ 2.56 MW per spill of 1.2 s and the average deposited power of ~ 355 kW over consecutive spills spaced by the SPS cycle of 7.2 s make the design of the proton target, its radiological protection, and its cooling very challenging aspects of the facility. Studies show that the required performance may be achieved with a longitudinally segmented hybrid target consisting of blocks of four nuclear interaction lengths (58 cm) of titanium-zirconium doped molybdenum alloy (TZM, density 10.22 g/cm^3 as compared to 10.28 g/cm^3 for pure Mo) in the core of the proton shower, followed by six nuclear interaction lengths (58 cm) of pure tungsten (density 19.3 g/cm^3). A medium-density material is required in the first half of the

2019 JINST 14 P03025

target in order to reduce the energy density and create acceptable stresses in the blocks. The blocks are all interleaved with 5 mm wide slots for water cooling. Tantalum alloy cladding of the TZM and the tungsten blocks is considered in order to prevent corrosion and erosion by the high flow rate of the water cooling. In order to respect the material limits derived from thermo-mechanical stresses, the thickness of each block together with the location of each cooling slot has been optimised to provide a relatively uniform energy deposition and sufficient energy extraction. Using FLUKA Monte Carlo simulations [17] and ANSYS finite element analyses, the preliminary target design has been shown to limit the peak power density in the target blocks to below 850 J/cm^3/spill and compressive stresses below 300 MPa in the core of the shower for a 6 mm RMS spot size and 30 mm single-turn sweep radius. Figure 11 (top) shows the preliminary proton target as designed for the SHiP Technical Proposal [1]. The total dimensions of the target are 1.2 m in length with transverse dimensions of 30 $\times$ 30 cm^2. Figure 11 (bottom) shows the maximum energy density per spill of $4 \cdot 10^{13}$ protons on target.

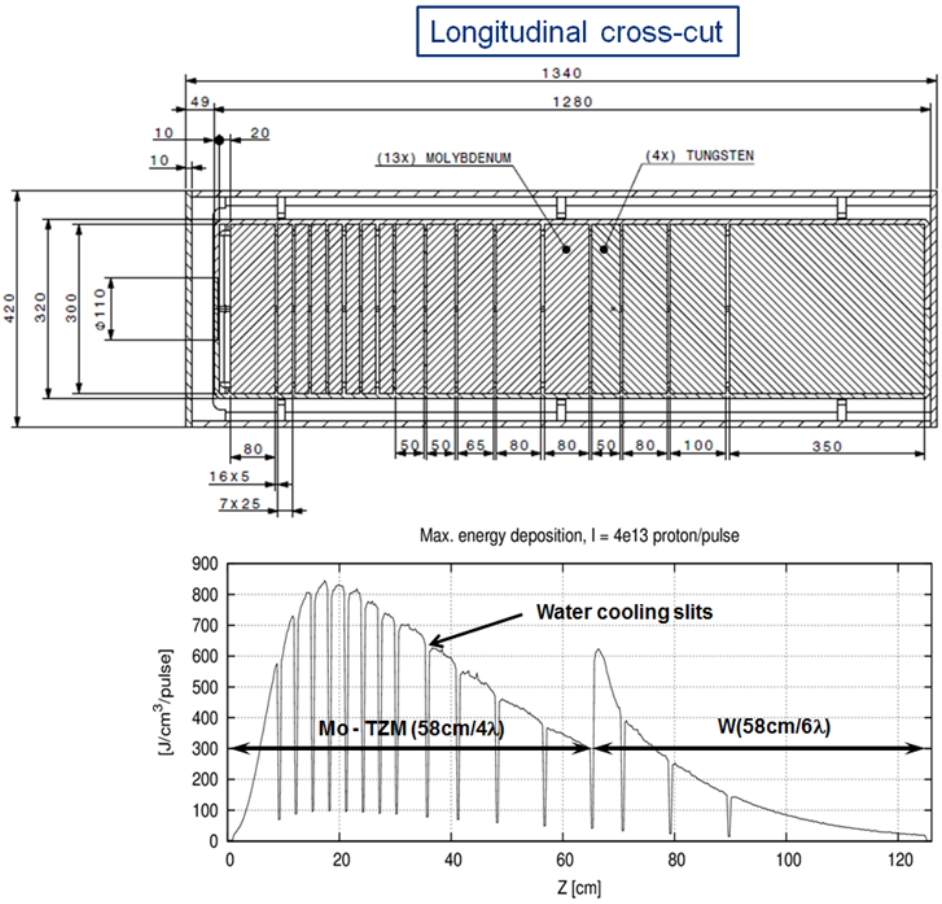

Figure 11. (Top) Preliminary design of the proton target configuration. All dimensions are in mm. The right-slanted hatched region in the top drawing shows the TZM blocks and the left-slanted hatched region the tungsten blocks. (Bottom) Peak energy deposition in the proton target during a spill of $4 \cdot 10^{13}$ protons.

Over the long term, the very high proton cumulated dose alters the physical and mechanical properties of the target material such as thermal conductivity and yield strength. First estimates of

2019 JINST 14 P03025

the radiation damage in terms of the displacement per atom, as well as the internal production of hydrogen and helium gas, indicate that the current target design ensures the longevity of the target, but the limited availability of data in literature call for accelerated aging studies of the materials with irradiation. A replica target is being designed and built for testing with beam in 2018.

The proton target blocks are assembled in a double-walled vessel. The inner vessel enforces the high-flow water circulation between the proton target blocks and ensures a pressurised water cooling of 15–20 bar in order to avoid water boiling in contact with the target blocks. A flow rate of $\sim 180\,\mathrm{m}^3/\mathrm{h}$ is envisaged. The outer vessel acts as a safety hull to contain hypothetical leaks, and is filled with an inert gas to prevent corrosion.

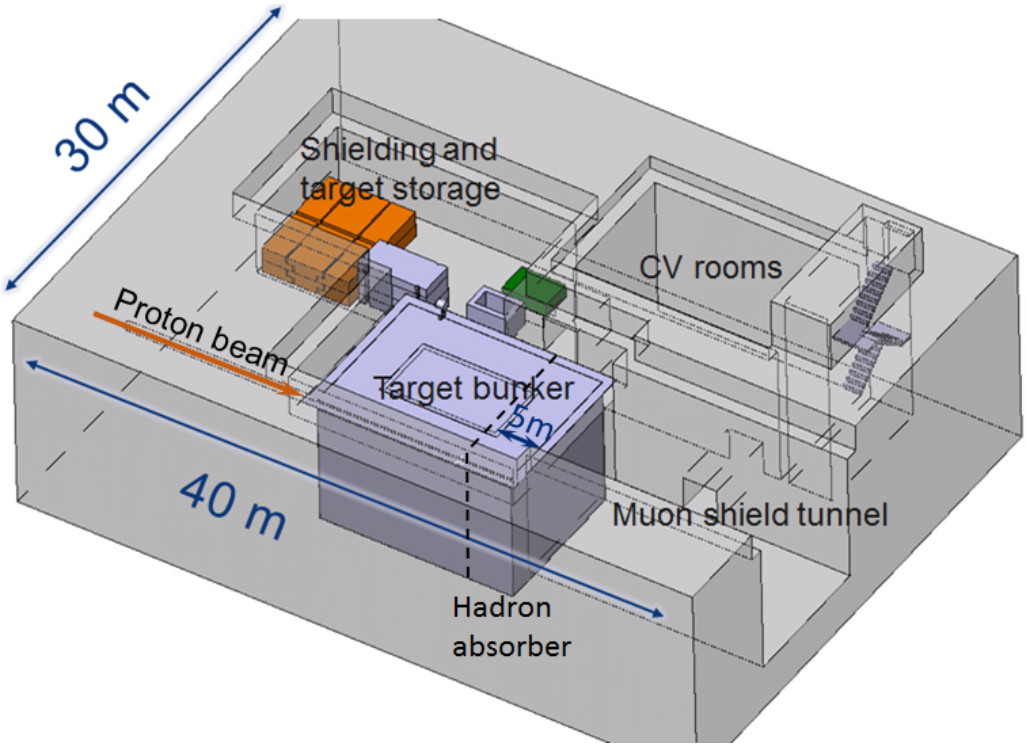

Figure 12. Overview of the main components of the target complex. The proton beam line arrives from the left of the target bunker. The target is located in the centre of the target bunker and the first section of the muon shield in terms of the magnetised hadron absorber is integrated in the downstream end of the bunker.

4.2 Preliminary design of the target complex

An overview of the target complex is shown in figure 12. In order to contain the radiation generated by the beam impacting on the proton target, the target is embedded in a $\sim 450\,\mathrm{m}^3$ cast-iron bunker. The inner part of the cast iron shielding ($\sim 20\,\mathrm{m}^3$) is water cooled by means of embedded stainless steel pipes in order to extract the average power of 20 kW which is leaking out of the target during operation. The outer part of the shielding is fully passive. The assembly has been designed with emphasis on reliability, remote handling and with the aim of being multi-purpose, i.e. allowing exchange of the proton target and the shielding configuration for alternative uses in future experiments. To minimise the irradiation of the primary beam line, the upstream shielding has only a

2019 JINST 14 P03025

limited passage of about 20 cm in diameter for the beam vacuum chamber. The 5 m thick downstream shielding acts as a hadron absorber with the double objective of absorbing the secondary hadrons and the residual non-interacting protons emerging from the target, and significantly reducing the exposure of the downstream active muon shield to radiation. The overall shielding is designed to respect the limits from radiological and environmental protection applicable at CERN.

A helium-vessel containing high-purity helium gas (> 99%) at atmospheric pressure encloses the SHiP proton target and the entire iron shielding. This is required to protect the equipment from radiation-accelerated corrosion as well as to avoid the production of high-mass radioactive isotopes from secondary neutrons interacting with air.

5 Suppression of beam-induced background

5.1 Active muon shield

The total flux of muons emerging from the proton target with a momentum larger than 1 GeV/c amounts to $O(10^{11})$ muons per spill of $4 \cdot 10^{13}$ protons. In order to control the background from random combinations of muons producing fake decay vertices in the detector decay volume and from muon deep inelastic scattering producing long-lived neutral particles in the surrounding material, and to respect the occupancy limits of the sub-detectors, the muon flux in the detector acceptance must be reduced by several orders of magnitude over the shortest possible distance. To this end, a muon shield entirely based on magnetic deflection has been developed [18, 19] (figure 1).

Figure 13 shows schematically the field configuration of the muon shield magnets. The first section of the muon shield starts within the hadron absorber with the integration of a coil which magnetises the iron shielding block, and continues with a set of freestanding magnets over a length of $\sim$ 20 m. The purpose of the first section is to deflect the positively and negatively charged muons on either side of the beam axis. As shown by the trajectories of the muons in figure 13, lower momentum muons and muons with larger transverse momenta are swept out of the core field before the end of the first section. Due to the return fields, a large fraction of these muons are bent back towards the detector acceptance. For this reason, the second section serves two purposes. In addition to providing further bending power to deflect out of acceptance the higher momentum muons, it should also give the lower momentum muons another magnetic kick outwards. This 20 m section therefore consists of a series of magnets with the return field close to the z-axis. The residual muons entering the decay volume after the muon shield are mainly due to stochastic processes involving large energy losses and large angle scattering in the muon shield material.

In order to achieve a high magnetic flux of 1.7–1.8 T in the core at low current and with coils of small cross-sections, grain-oriented steel is considered as the yoke material for the freestanding magnets [18]. The actual field configuration for the entire muon shield has been optimised with the help of machine learning techniques using a large sample of muons from a full GEANT4 [20] simulation of $2 \cdot 10^{10}$ protons on the SHiP proton target. Engineering studies are underway to study the optimal assembly techniques. The total mass of the muon shield magnets is of the order of 1500 tonnes. The current design allows reducing the rate of residual muons above 1 GeV/c reconstructed in the SHiP spectrometer to an acceptable rate of $O(10^5)$ per spill.

2019 JINST 14 P03025

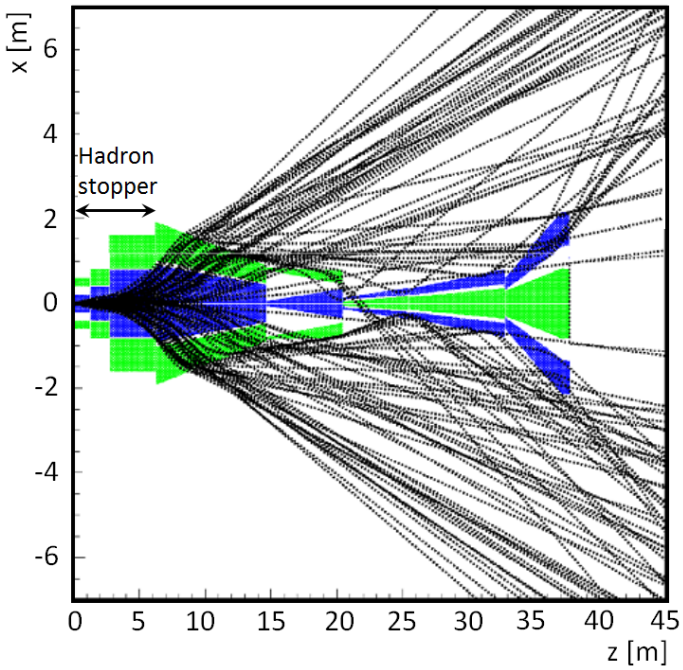

Figure 13. Horizontal cross-section of the muon shield magnet configuration at the level of the beam-axis. The direction up/down of the vertical magnetic field is illustrated by the blue/green colour of the iron poles of the magnets. Typical trajectories of muons across the momentum spectrum are overlaid. Reproduced from [19]. CC BY 3.0.

5.2 Vacuum vessel

Deep inelastic neutrino-nucleon scattering in the detector volume leads to background events through the production of V^0 particles (K_L, K_S, Λ) whose decay mimic the topology and modes of the hidden particle decays. With $2 \cdot 10^{20}$ protons on target, a flux of $\sim 4.5 \cdot 10^{18}$ neutrinos and $\sim 3 \cdot 10^{18}$ anti-neutrinos are expected within the angular acceptance of the SHiP detector. The flux is dominated by muon neutrinos coming from the decays of pions and kaons produced in the proton target. Neutrinos from decays of charm and beauty hadrons constitute $\sim 10\%$ of the total neutrino flux. Figure 14 (left) shows the vertex distribution of signal candidates produced by neutrino interactions assuming air at atmospheric pressure in the fiducial volume, and no surrounding vessel structure. A soft selection for heavy neutral leptons based on finding a vertex in the fiducial volume and no activity in the upstream detectors is applied. In these conditions, a total number of $2.5 \cdot 10^3$ candidate events are expected within the acceptance for $2 \cdot 10^{20}$ protons on target. The events are largely concentrated along the centre with small reconstructed impact parameters at the proton target. To achieve the required level of neutrino background rejection, the fiducial volume is therefore contained in a vacuum vessel (figure 1) which is evacuated down to a pressure of $O(10^{-3})$ bar. Figure 14 (right) shows the vertex distribution of signal candidates at this pressure. In these conditions, $1.4 \cdot 10^4$ candidate events are expected within the fiducial volume with the same soft selection for $2 \cdot 10^{20}$ protons on target, mainly produced through neutrino interactions with the vessel walls. Even if the total number of neutrino interactions are larger due to the vessel material, almost all candidate events are in this case easily rejected by using criteria based on the reconstructed impact parameter at the

2019 JINST 14 P03025

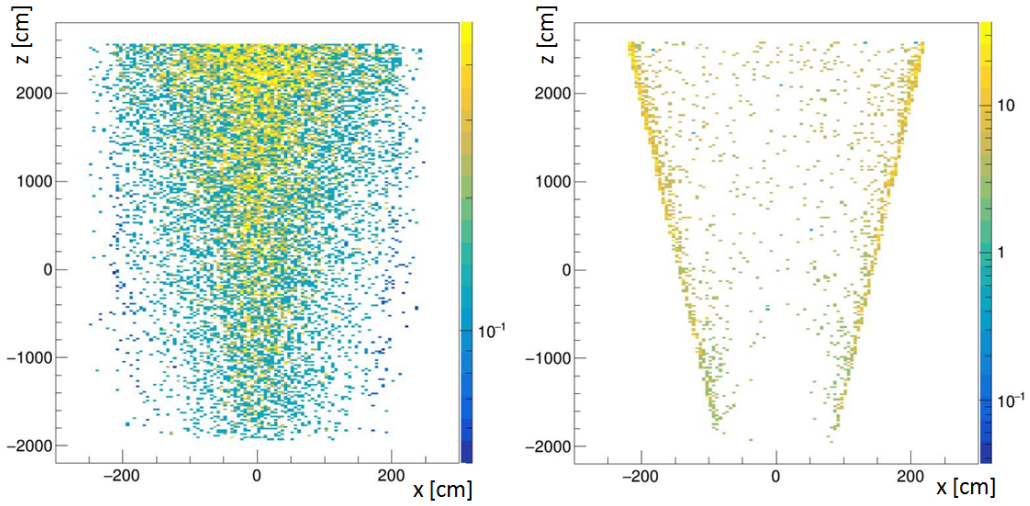

Figure 14. Vertex distribution of signal candidates produced by neutrino interactions from $2 \cdot 10^{20}$ protons on target assuming air at atmospheric pressure in the fiducial volume with a soft selection for heavy neutral leptons (left), as compared to the situation with a vacuum vessel evacuated down to a pressure of 10^{-3} bar (right).

proton target. In addition, residual neutrino interactions as well as muon deep inelastic interactions with the vessel structure are further suppressed by instrumenting the entire decay volume walls with a background tagger system and detecting the additional activity associated with the interactions. Simulation studies show that no background events remain after applying these criteria [1].

The SHiP decay vessel consists of the ~ 50 m decay volume constructed in S355JO(J2/K2)W Corten steel with upstream outer dimensions of $2.4 \times 4.5\,\mathrm{m}^2$ and downstream outer dimensions of $5 \times 10\,\mathrm{m}^2$. The design of the vessel wall is based on an optimisation aiming at producing a structure as light as possible and as slim as possible in order to stay within the boundaries of the deflected muon flux whilst maintaining the required acceptance. At the same time, the optimisation also accounts for the structural safety norms allowing access to the underground hall while under vacuum and the earthquake loads in the region. Figure 15 shows the structure of the decay volume. The preliminary design consists of a 30 mm thick continuous inner steel sheet acting as vacuum liner, supported azimuthally by welded T-shaped beams with a steel thickness of 15 mm and a height varying from 300 mm to 450 mm. The structure is further reinforced by longitudinal stiffening profiles between the azimuthal beams.

Two options are considered for the surrounding background tagger, either a liquid or a plastic scintillator. For the liquid option, the scintillator is integrated within the decay volume structure with an extra 8 mm steel sheet welded to the azimuthal beams and stiffening profiles, while for the plastic scintillator option, it is attached directly to the structure. The decay volume is directly connected to the ~ 10 m downstream spectrometer vacuum section, which is made out of austenitic steel since it runs through the spectrometer magnet and houses the four tracker stations of straw tubes built using the same technology from the NA62 experiment [21]. The preliminary design considers extruded aluminum profiles with a material budget equivalent to 0.8 radiation lengths for the upstream and downstream windows.

2019 JINST 14 P03025

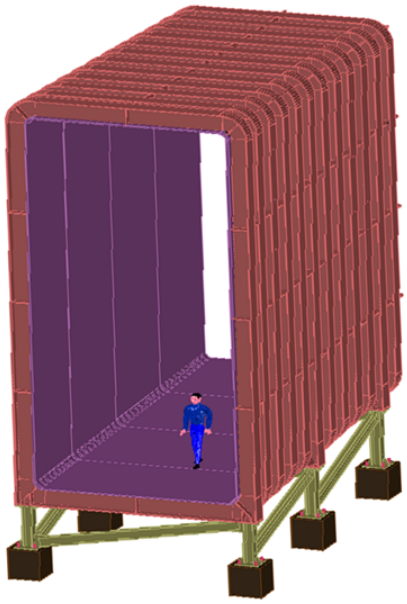

Figure 15. Cross-sectional view of the vacuum vessel which provides a pressure of $O(10^{-3})$ bar in the decay volume. The design has been optimised in order for the wall to be as light and as slim as possible, and to incorporate a detector system which tags background events.

6 Conclusions

The SHiP experimental facility will provide a unique experimental platform for physics at the intensity frontier which is complementary to both the searches for new physics at the energy frontier and the direct searches for cosmic Dark Matter. CERN's accelerator complex makes for an ideal siting for the experimental facility. The assumed availability of $2 \cdot 10^{20}$ protons on target at 400 GeV/c in about five years of nominal operation and an environment of extremely low background compares favourably with the potential of other existing facilities.

The two-fold SHiP apparatus is sensitive both to decays and to scattering signatures, and is able to probe a wide variety of models with light long-lived exotic particles in a largely unexplored domain of very weak couplings and masses up to $O(10)$ GeV/c^2. This puts it in a unique position worldwide to resolve several of the major observational puzzles of particle physics and cosmology. In addition, the same facility enables the study of interactions of tau neutrino and anti-tau neutrinos, as well as neutrino-induced charm production by all neutrino species. A more recent investigation also shows that an additional detector on the SHiP beam line with a proton target consisting of thin wires and operating in parallel would allow a search for lepton flavour violating tau lepton decays at a sensitivity that could be highly competitive with projections of approved experiments.

The experimental facility presents a number of technological challenges to the beam delivery, the proton target system, and the reduction of beam-induced background. As reported, in-depth studies and prototyping are already well underway for all of the critical components. Taking into account the required R&D and construction, and the accelerator schedule at CERN, we plan to commission and perform the pilot run for the SHiP experiment when the SPS resumes operation after LHC's third long shutdown for maintenance and upgrades.

2019 JINST 14 P03025

Acknowledgments

The SHiP Collaboration wishes to thank the Castaldo company (Naples, Italy) for their contribution to the development studies of the decay vessel. The support from the National Research Foundation of Korea with grant numbers of 2018R1A2B2007757, 2018R1D1A3B07050649, 2018R1D1A1B07050701, 2017R1D1A1B03036042, 2017R1A6A3A01075752, 2016R1A2B40-12302, and 2016R1A6A3A11930680 is acknowledged. The support from the Russian Foundation for Basic Research, grant 17-02-00607, and the support from the TAEK of Turkey are acknowledged.

References

[1] SHiP collaboration, *A facility to Search for Hidden Particles (SHiP) at the CERN SPS*, arXiv:1504.04956.

[2] S. Alekhin et al., *A facility to Search for Hidden Particles at the CERN SPS: the SHiP physics case*, *Rept. Prog. Phys.* **79** (2016) 124201 [arXiv:1504.04855].

[3] SHiP collaboration, *Addendum to Technical Proposal: A Facility to Search for Hidden Particles (SHiP) at the CERN SPS*, CERN-SPSC-2015-040 (2015).

[4] G.F. Giudice and R. Rattazzi, *Theories with gauge mediated supersymmetry breaking*, *Phys. Rept.* **322** (1999) 419 [hep-ph/9801271].

[5] I. Yu. Kobzarev, L.B. Okun and I. Ya. Pomeranchuk, *On the possibility of experimental observation of mirror particles*, *Sov. J. Nucl. Phys.* **3** (1966) 837.

[6] R. Foot, H. Lew and R.R. Volkas, *A Model with fundamental improper space-time symmetries*, *Phys. Lett.* **B 272** (1991) 67.

[7] R. Foot and X.-G. He, *Comment on Z Z-prime mixing in extended gauge theories*, *Phys. Lett.* **B 267** (1991) 509.

[8] B. Patt and F. Wilczek, *Higgs-field portal into hidden sectors*, hep-ph/0605188.

[9] R. Essig et al., *Working Group Report: New Light Weakly Coupled Particles*, in *Proceedings of the 2013 Community Summer Study on the Future of U.S. Particle Physics*, Snowmass on the Mississippi, Minneapolis, MN, U.S.A., 29 July–6 August, 2013, arXiv:1311.0029, http://www.slac.stanford.edu/econf/C1307292/docs/IntensityFrontier/NewLight-17.pdf.

[10] J. Alexander et al., *Dark Sectors 2016 Workshop: Community Report*, arXiv:1608.08632, FERMILAB-CONF-16-421 (2016).

[11] OPERA collaboration, *The OPERA experiment in the CERN to Gran Sasso neutrino beam*, 2009 *JINST* **4** P04018.

[12] E. Gschwendtner et al., *CNGS, CERN Neutrinos to Gran Sasso, five years of running a 500 kilowatt neutrino beam facility at CERN*, in *Proceedings of IPAC2013*, Shanghai, China, 12–17 May 2013, pp. 211–213.

[13] K. Elsener, G. Fidecaro, M. Gyr, W. Herr, J. Klem, U. Mikkelsen et al., *Proton extraction from the CERN SPS using bent silicon crystals*, *Nucl. Instrum. Meth.* **B 119** (1996) 215.

[14] COMPASS collaboration, http://wwwcompass.cern.ch/.

[15] L.R. Evans et al., *The steel septum magnets for beam splitting at the CERN SPS*, in *Proceedings of the 6th International Conference on Magnet Technology (MT-6)*, Bratislava, Slovakia, 29 August–2 September 1977 [CERN-SPS-ABT-77-13].

2019 JINST 14 P03025

[16] H. Dijkstra and T. Ruf, *Heavy Flavour Cascade Production in a Beam Dump*, CERN-SHiP-NOTE-2015-009 (2015).

[17] A. Ferrari, P.R. Sala, A. Fasso and J. Ranft, *FLUKA: A multi-particle transport code (Program version 2005)*, CERN-2005-010, SLAC-R-773, INFN-TC-05-11 (2005).

[18] V. Bayliss, M. Courthold and T. Rawlings, *Active Muon Shield - Preliminary Design Report*, CERN-SHiP-NOTE-2015-003 (2015).

[19] SHiP collaboration, *The active muon shield in the SHiP experiment*, 2017 *JINST* **12** P05011 [arXiv:1703.03612].

[20] GEANT4 collaboration, *GEANT4: A Simulation toolkit*, *Nucl. Instrum. Meth.* **A 506** (2003) 250.

[21] G. Anelli et al., *Proposal to measure the rare decay $K^+ \to \pi^+ \nu\bar{\nu}$ at the CERN SPS*, CERN-SPSC-2005-013 (2005).

2019 JINST 14 P03025